Emergent behavior in particle-laden microfluidic systems informs strategies for improving cell and particle separations

Citation: Vahey, Michael D., and Joel Voldman. Emergent Behavior in Particle-laden Microfluidic Systems Informs Strategies for Improving Cell and Particle Separations. Lab on a Chip 11, no. 12 (2011): 2071.

As Published: http://dx.doi.org/10.1039/c0lc00602e

Publisher: Royal Society of Chemistry, The

Persistent URL: http://hdl.handle.net/1721.1/80788

Version: Author's final manuscript: final author's manuscript post peer review, without publisher's formatting or copy editing

Emergent behavior in particle-laden microfluidic systems informs strategies for improving cell and particle separations

*Michael D. Vahey and Joel Voldman**
Department of Electrical Engineering and Computer Science, 77 Massachusetts Avenue, Building 36-824, Cambridge, Massachusetts 02139
voldman@mit.edu*

Abstract
Colloidal particles placed in an energy landscape interact with each other, giving rise to complex dynamic behavior that affects the ability to process and manipulate suspensions of these particles. Propagating across scales ranging from the local behavior of 10's of particles to non-local behavior encompassing $>10^6$ particles, these particle interactions are pervasive and challenging to describe quantitatively, especially in the confined environments typical of microfluidic devices. To better understand the effects of particle interactions in this context, we have performed experiments and simulations involving a simple microfluidic device in which hydrodynamic and electrostatic forces are leveraged to concentrate and separate particle mixtures. These investigations reveal the mechanisms underlying the dynamic patterns formed by micron-scale particles as they impinge on a dielectrophoretic force barrier: their tendency to aggregate and recirculate under constant operating conditions, and to reorganize when the operating conditions are changed. The emergent behaviors of these ensembles of interacting particles exhibit features of dynamical frustration and cooperativity that suggest non-intuitive strategies for concentrating and sorting suspensions. Finally, we present a simple analytic model based on hydrodynamic coupling that captures important features of strongly interacting particle suspensions.

Introduction
The control and manipulation of particles and cells has become a fundamental application of microfluidic technology, in contexts including cell enrichment and purification[1, 2], droplet/bubble generation and control[3-5], and sample preparation[6, 7], among others. The devices developed for these applications typically process many particles at once, yet the models and intuition used in their design usually consider a single, isolated particle in the system. Although the pervasiveness and potential significance of physical interactions between particles is often recognized[8-10] – and in some cases leveraged to achieve systems that self-organize[11, 12] - the challenge of incorporating their effects into the general design of microfluidic devices remains largely unresolved. This challenge is magnified by a general characteristic of systems with many interacting components: the emergence of complex, unexpected behavior. Some of these behaviors include pattern formation[13-15], cooperativity[16-18], hysteresis[19], synchronization[20, 21], and frustration[22-24], and may arise in microfluidic devices under appropriate conditions. Although previous work regarding particle interactions in microfluidic devices has dealt with electrostatic interactions and particle aggregation under static conditions[25] (i.e. no hydrodynamic interactions), developed continuum theories[26, 27], or focused on the rigorous calculation of the trajectories of specific arrangements of interacting particles[28], the propagating effects of particle interactions across increasingly large scales (*i.e.*, from a few to many thousands of particles) and the collective behavior they give rise to – in particular, their dynamical patterns, cooperativity, hysteresis and frustration - remains unexplored in a practical context. Connecting an understanding of how particles interact at an atomistic level to device operation at a more macroscopic level would facilitate predicting how a device will operate at concentrations exceeding infinite dilution.

To better understand and predictively quantify the influence of particle interactions on the performance of microfluidic devices, we have developed experiments, dynamic simulations, and a statistical model. This multifaceted approach provides a simple and versatile platform for studying collective behaviors and emergence in multi-particle microfluidic systems. While many types of

interaction forces can arise in microfluidics applications - for example, electrical, magnetic, optical, or hydrodynamic forces, both between particles coupling with each other directly as well as through their images in the system's boundaries[29], - we have chosen to specifically study the behavior of electric and hydrodynamic interactions. Hydrodynamic forces are ubiquitous in microfluidic systems, while electrical forces are important (*i.e.*, widely used[30, 31]), experimentally convenient (*i.e.*, easy to modulate), and anisotropic, giving rise to more complex patterns. By observing the dynamics of one to thousands of particles simultaneously in a canonical microfluidic device that combines a microchannel with interdigitated electrodes, we are able to understand - through numerical and statistical models - the patterns that arise between interacting particles due to the hydrodynamic and electrical forces. Through this combined experimental and computational approach, we provide insight into how particle interactions can be leveraged to design higher-performance microfluidic devices.

Results

Particle Aggregates: Dynamical Patterns. To study particle interactions, we used a shallow microfluidic channel overlaying a microfabricated array of interdigitated electrodes, through which we flowed particles perpendicular to the axis of the electrodes (Figure 1*a*). In operation, an AC voltage was applied across the electrodes, polarizing particles and exerting a negative dielectrophoretic force; this force counteracts hydrodynamic drag, retaining the particles if the voltage is large enough. The frequency of the electric field (≥1 MHz) and size of the particles (~1-4μm in diameter) were chosen to minimize the significance of thermal forces, as well as electrophoretic effects sensitive to the charge and zeta potential of the particles.

In the case of an isolated particle impinging upon the electrodes, the dielectrophoretic force required to overcome drag is given by the balance of the two forces, and can be readily calculated. However, in highly concentrated suspensions, we observed particle aggregations whose formation and behavior exhibited a stochastic dependence on the applied voltage, flowrate, and the number of interacting particles. We used experiments and simulations to study these patterns, observing 1- to 4-μm-diameter colloidal particles in the presence of externally imposed electric and hydrodynamic fields. We repeatedly observed a variety of behaviors that varied as the number of particles entrained in the aggregate increased.

As aggregates of a few to several particles begin to assemble, they take the form of chains aligned to the electric field, commonly known as "pearl chains"[32]. As a result of hydrodynamic interactions, these chains experience less drag per particle than single particles in isolation[33], and entrain incoming particles through dipole interactions[32]. As the chains lengthen, disturbances to the back of the chain allow bifurcations to form, giving rise to branching particle chains (resembling an inverted 'Y' shape; Figure 1*b*). A second response we observed in lengthening chains was the detachment of particles from the weakly polarized back end, which were then carried forward by flow, where they rejoined the strongly polarized front end of the chain, producing a periodic "treadmilling" behavior (Figure 1*c*, supplementary video S1). Finally, as the particle aggregate grew increasingly large, the chain structure was lost in favor of a closely packed cluster of particles which continually recirculated under hydrodynamic forces (Figure 1*d*, supplementary video S2).

We used three-dimensional numerical Brownian and Stokesian dynamics simulations[34, 35] to determine the set of physical interactions necessary to capture the observed behaviors. In the simulations, we first specified the imposed electric field, $\mathbf{E}_0$, and fluid velocity, $\mathbf{u}_0$, together with the positions of N interacting particles, $\mathbf{x}_i(t)$ ($i = 1 \ldots N$). To self-consistently determine the electric and hydrodynamic fields given each particle's position, polarization, and velocity relative to the surrounding medium, we used:

$$\mathbf{E}(\mathbf{x}) = \mathbf{E}_0(\mathbf{x}) + \sum_{\mathbf{i}=1\ldots\mathbf{N}} \mathbf{G}_{\text{ES}}(\mathbf{x};\mathbf{x_i})\mathbf{E}(\mathbf{x_i}) \tag{1a}$$

$$\mathbf{v}(\mathbf{x}) = \mathbf{u}_0(\mathbf{x}) + \sum_{\mathbf{i}=1\ldots\mathbf{N}} \mathbf{G}_{\text{HD}}(\mathbf{x};\mathbf{x_i})\mathbf{F}(\mathbf{x_i}) \tag{1b}$$

Here, $\mathbf{F}(\mathbf{x}_i)$ denotes the net external force acting on the i^{th} particle, and the Green's functions $\mathbf{G}_{\text{ES}}$ and $\mathbf{G}_{\text{HD}}$ represent electrostatic and hydrodynamic coupling between particles and to the system's boundaries[36]. Given the self-consistent electric field ($\mathbf{E}$), the dielectrophoretic contribution to the external force is given by:

$$\mathbf{F_i} = \mathbf{p_i} \cdot \nabla \mathbf{E}(\mathbf{x_i}) = 4\pi\varepsilon_m a_i^3 K_i \left[\mathbf{E}(\mathbf{x_i}) \cdot \nabla \mathbf{E}(\mathbf{x_i})\right] \tag{2}$$

where a_i and K_i denote the radius and polarizability of the i^{th} particle, respectively. In addition, the net external force contains a steric contribution, preventing overlap between contacting particles and/or surfaces. Using the net force, we calculated the velocity of each particle using:

$$\mathbf{v_j^p} = \mathbf{u}_0(\mathbf{x_j}) + (6\pi\mu a_i)^{-1}\mathbf{F}(\mathbf{x_i}) + \sum_{\mathbf{i}=1}^{\mathbf{N}} \mathbf{G}_{\text{HD}}(\mathbf{x_j};\mathbf{x_i})\mathbf{F}(\mathbf{x_i}) \tag{3}$$

Although our simulations consider systems in which thermal and electrophoretic forces are negligible relative to dielectrophoretic and hydrodynamic drag forces (*i.e.* high electric field frequency and particles with low diffusivity), generalizing equation (2) to include these effects presents no fundamental obstacle.

Using these simulations, we were able to recapitulate the experimentally observed behaviors (Figure 1*b-d*, supplementary video S1-2). The agreement between simulations and experiments suggests that our modeling approach captures the essential physical aspects of large (>1 μm) interacting colloidal particles in high-frequency (>1 MHz) electric fields. This agreement in turn allowed us to investigate the minimal set of interaction rules necessary to reproduce the experimentally observed behaviors. Using simulations, we are able to selectively turn on or off different types of coupling between particles and examine the consequences. For example, we found that removing hydrodynamic interactions (but not the external hydrodynamic field) from the simulations resulted in the loss of the dynamic patterns from Figure 1*c*&*d*, such that particle chains emerged but no treadmilling was observed (Figure 1*e*, "ES only"). In contrast, the selective removal of electrostatic (but not hydrodynamic) interactions recaptured the dynamics of large aggregates, but without particle chains (Figure 1*e*, "HD only"). Accordingly, we found that inclusion of *both* hydrodynamic and electrostatic interactions was essential to accurately reproduce the system's behavior (Figure 1*e*, "HD & ES"). Interestingly, we observed that removal of electrostatic coupling (Figure 1*e*, "HD only") much more closely resembles the full simulation (Figure 1*e*, "HD & ES") than does the selective removal of hydrodynamic coupling (Figure 1*e*, "ES only"); without hydrodynamic interactions, the aggregates essentially freeze into a stable configuration with very little subsequent dynamics (Supplemental movie S3). This discrepancy with respect to both simulations and experimental observations suggests that including hydrodynamic interactions in device modeling may be particularly important in many cases.

Particle Aggregates: Cooperative Nucleation. Although the dynamics of several interacting particles depends subtly on the balance between different types of interactions and requires numerical analysis, we wanted to explore the initial formation of a particle aggregate, to determine if this simpler situation could be quantitatively understood in terms of an analytical model. For this, we hypothesized that the collective behavior we observed on the scale of ~1-10 particles was initiated by fluctuations in the local particle concentration; when several particles approached the electrode barrier in close proximity, hydrodynamic and electrical interactions between them resulted in their retention by the barrier as an aggregate, even in cases where the force was not sufficiently strong to retain them as isolated particles. These "nucleation" events occur with a probability that depends on the concentration of particles impinging on the barrier (c) as well as the magnitude of the external electrical force (F_{ES}). Additionally, this nucleus of particles can continue to grow, retaining an increasing proportion of the incoming particles

over time and dramatically influencing such "macroscopic" properties of device operation as the performance of a particle concentrator or separator. To study the implications of particle interactions on a scale directly relevant to device performance, we performed experiments to determine how the external force necessary to observe nucleation within a fixed time frame varies with the concentration of particles entering the device, and developed a probabilistic model to describe the nucleation process.

Figure 2*a* schematically illustrates the model, consisting of a particle surrounded by N neighbors with which it interacts. We assume that the contribution to the interaction force (= f) of any of these N particles is randomly distributed according to $p(f) = 4\log(h/a)e^{-4\log(h/a)f/F_{ES}}$ (where h denotes the channel height and a denotes the particle radius; see Supplementary Information for a discussion of this expression). In all of the following, we treat the external and interaction forces as scalars, acting opposite the direction of hydrodynamic drag. This assumption simplifies the model considerably and is consistent with an isotropic, uniformly distributed suspension of particles, acted upon by forces that are uniform when averaged over a large volume.

Nucleation occurs when statistical fluctuations in N and f give rise to a total force acting on a particle that is sufficiently strong to retain it against the imposed fluid velocity (U). For a given concentration c (units of m^{-3}), we found that the distribution of N is accurately approximated by $p[N] = [(4\pi h^3 c)^N/N!]e^{-4\pi h^3 c}$. This combined with $p(f)$ allows us to determine the distribution of the net interaction force, $p(f_{net})$, experienced by a particle as a function of the global concentration and externally applied force (see Supplementary Information for derivation). From this result, we are able to determine the probability that a given particle will form a nucleation site by evaluating the integral $p_{nuc} = 1 - \int_0^{(F_{HD}-F_{ES})/F_{ES}} p(f_{net}/F_{ES})\,d(f_{net}/F_{ES})$. Here, F_{HD} denotes the magnitude of the drag force, and thus the force that must be overcome to retain a particle. Since $p(f_{net}) = 0$ for $f_{net} < 0$, if $F_{HD} \le F_{ES}$ then the external electrical force is strong enough to retain a single particle, resulting in $p_{nuc} = 1$; this corresponds to every particle acting as a nucleation site, which is the case when the dielectrophoretic force is strong enough to retain every particle.

Although there is no closed-form expression for the integral for p_{nuc}, if the external applied force is sufficiently weak, we determined that p_{nuc} could be approximated by a general sigmoidal function in the form of a Hill equation, analogous to cooperative binding:

$$p_{nuc} \approx \frac{c^n}{K_D^n + c^n} \tag{4}$$

In terms of the forces present in the system, the effective dissociation constant, K_D, and the effective Hill coefficient, n, can be approximated by (discussed in Supplementary Information):

$$\begin{aligned} K_D &\approx \left(\log(h/a)/\pi h^3\right)\left[(F_{HD}/F_{ES}) - 1\right] \\ n &\approx 2\sqrt{4/\pi\left[(F_{HD}/F_{ES}) - 1\right]\log(h/a) + (\log 2)^2} \end{aligned} \tag{5}$$

An intuitive link can be drawn between hydrodynamic interactions and cooperative binding. Similar to how the presence of one molecule occupying a binding site increases the affinity of subsequent molecules to bind in adjacent cites, the disruption one particle creates in the surrounding hydrodynamic field increases the likelihood that other particles in close proximity will be retained. In both cases, the mechanism can be thought of as a particle distorting its surrounding environment (through allosteric effects and conformational changes in the molecular analogy, and through hydrodynamics in the case of colloids) so as to encourage the recruitment of other particles. In the context of cooperative binding, n = 1 implies no cooperativity, with $n > 1$ indicating positive cooperativity. In our case, as the applied force F_{ES} decreases, the ability to retain particles becomes more sensitive to the number of particles interacting with each other, increasing cooperativity and hence n. The lower limit for n in this model, approached as $F_{ES} \to F_{HD}$, is $2\log 2$ (≈ 1.39) – comparable with but not equal to the case of no cooperativity, a difference likely attributable to the simplifications inherent in the model.

Given the nucleation probability for a single particle, the probability that one or more nucleation events will occur is $1 - (1 - p_{nuc})^{Qct}$. Here, Q gives the volumetric flow rate and t gives the operating duration, so that the total number of particles passing through the device is Qct. A nucleation event can be expected to occur once p_{nuc} is comparable to $[Qct]^{-1}$. Combining this result with equations (4) and (5) provides a means of determining the external force at which nucleation can be expected to begin for a given particle concentration.

To experimentally test this model, we introduced different concentrations of particles into the coplanar electrode device and determined the threshold voltage at which nucleation would occur within t =300 s (Figure 2*b*). We observed that at very low particle concentrations (low c), the threshold voltage approximated that expected for isolated particles (no interaction forces), but that there was a sharp decrease in the threshold force as c increased, followed by a slower decrease in the force needed for nucleation as the concentration increased further. Both of these trends were recapitulated by the model. Importantly, our model predicts that the force-concentration relationship for nucleation will scale weakly with time for sufficiently large t. For a given external force, the concentration at which nucleation will initiate scales as $t^{-1/(n+1)}$, where $n \geq 1.39$. As a result, our experimental results (obtained using an operating duration of 300 s) are largely insensitive to the exact interval of time chosen. For example, at a concentration of 10^{14} particles/m^3, increasing the duration by one order of magnitude (from 300 s to 3000 s) is expected to decrease the force threshold by ~10%. Accordingly, nucleation tends to occur at early times and at low concentrations. This suggests that an "infinitely dilute" operating regime may be experimentally challenging to achieve in many applications, and highlights the importance of modeling particle interactions in order to accurately understand device behavior.

Viewing particle interactions in the context of cooperative binding leads to the hypothesis that because the force threshold for retaining particles decreases with increasing particle concentration, devices for handling concentrated suspensions should exhibit hysteresis. To test this hypothesis, we applied a time series of increasing and then decreasing voltages (slow enough to reach steady state) to our coplanar electrode system as we flowed in particles at a single concentration (Figure 2*c*). As we increased voltage, the size of the aggregate increased, as expected given the increasing electrostatic force. Upon decreasing voltage, the size of the aggregate decreased. Critically, however, the number of particles reached a different (higher) steady state, exhibiting a hysteretic loop. This observation of path dependence in colloidal systems follows directly from the nucleation-based model for particle aggregation (where higher concentrations make particle entrainment more likely), and can account for a wide variety of concentration-dependent effects observed in microfluidic devices. To develop this idea further, we explored more complicated scenarios involving mixtures of different types of particles.

Separations of Interacting Particles. While cooperation between particles is advantageous in making a relatively dilute suspension more concentrated, it generally has adverse effects on separations, where the objective is to *remove* components of a (concentrated) mixture, requiring the different components to exhibit different behavior (i.e., trapped vs. released) in a common environment. Based on our observation that concentrated suspensions exhibit hysteresis when they are acted on by electric and hydrodynamic fields, we hypothesized that separations could be influenced by using operating conditions that vary over time. In dielectrophoretic systems, a convenient way to vary the operating conditions is through the applied voltage (V) or by varying the electric field frequency (ω), which affects the particle polarizability, $K(\omega)$.

To explore how time-dependent operating conditions influence the performance of a separation, we performed experiments and simulations involving polystyrene beads with different sizes and polarizabilities. In these experiments, we introduced a mixture of two particles types into a coplanar device, subjected to conditions under which both components were retained, forming an aggegrate comprised of both particle types (Figure 3). Then, we suddenly varied the operating conditions (either applied voltage or particle polarizability, experimentally controlled through the electric field frequency). In both cases, we changed the voltage or frequency such that one particle type would ideally be retained

(in this case the green particles, 1.6 μm diameter), while the other particle type (the red particles, 1.0 μm diameter) would normally (in the dilute limit) not be retained. When the voltage was decreased, the external and interaction forces decreased proportionally. We observed that the dissociation of the particle cluster was incomplete, with the loss of desired (green) particles as well as the retention of undesired particles (red) (Figure 3*a*, supplementary video S4). Alternatively, varying the frequency, which affects the polarizability of the undesired particles (a change in K from -0.46 to ~0) considerably more than the desired particles (a change from -0.48 to -0.36), resulted in higher purity separation (Figure 3*b*, supplementary video S5). These results are likely attributable to the different scaling of the external and interaction forces with polarizability. Specifically, the external dielectrophoretic force acting on a particle scales proportional to KV^2, whereas the interaction force between two particles scales approximately as K^2V^2. As a result, reducing K has a proportionally larger effect on the strength of interactions between particles than on the external force acting on any given particle; as $K \rightarrow 0$, the interaction force is preferentially suppressed relative to the external force, whereas when $V \rightarrow 0$, the relative strength of interaction and external forces arising from the electric field remain constant. Thus, the two experiments above reflect how preferentially changing the interaction force (Figure 3*b*) results in improved purity over changed interaction and external force (Figure 3*a*). The implications of this scaling present an important consideration in the development of dielectrophoretic separation methods, suggesting that approaches that separate particles by varying polarizability will have improved purity and recovery over those that separate by varying voltage or flowrate.

We used numerical simulations with conditions matching these experiments and were able to recapitulate our observations when the polarizability and voltage are varied (Figure 3*a* & *b*, bottom panels). This quantitative agreement suggests that our simulations are able to predict separation dynamics, and thus can be used to study situations that are difficult to realize experimentally. Unlike the experiments in Figure 3, we can simulate cases where polarizability and voltage are varied in a way that changes the external electrical force identically in both cases. To do this, we considered binary separations operating under either constant conditions, time-varying polarizability, or time-varying voltage (Figure 4). Under constant conditions, we can operate at conditions *between* the trapping threshold for the two particles at infinite dilution (labeled '1' in Figure 4), or *beneath* the trapping thresholds at infinite dilution (labeled '3' and '5'). In this first situation ('1'), the desired particles would ideally be trapped and the undesired particles separated (in the absence of interactions), while in situations '3' and '5', neither particle would be trapped without interaction forces. We computationally introduced 100 particles of each type into the device and modeled the time evolution of the retention of each particle type, allowing determination of the purity (the fraction of retained particles that were desired) and recovery (i.e. the fraction of desired particles that were retained). Constant operating conditions between the thresholds resulted in high recovery but low purity, because a significant number of undesired particles were retained as the concentration increased (Figure 4*c*, row 1). Alternatively, constant operating conditions beneath both trapping thresholds at infinite dilution achieved high purity but low recovery, since the majority of particles were not retained (Figure 4*c*, rows 3 and 5).

An alternate separation approach is to vary the operating conditions over time, so as to stay approximately between the trapping thresholds as the concentration changes. This can be accomplished by varying either the polarizability (labeled '2' in Figure 4), or the applied voltage (labeled '4'). In both cases, time-varying conditions improve the composite purity/recovery (as determined by the geometric mean) relative to constant operating conditions. The improvement is particularly pronounced when the polarizability was varied (Figure 4*c*, row 2), consistent with the scaling of forces with voltage and polarizability; because the external electrical forces scale relative to electrical interactions as $\sim K^{-1}$, lowering the polarizability led to greater disaggregation in a mixture of closely coupled particles, and thus higher purity separation. Accordingly, the superior performance of separations based on varying polarizability (Figure 4*a*, supplementary video S6) as opposed to varying voltage (Figure 4*b*, supplementary video S7) derives from the ability to leverage interactions between particles when they are

desirable (i.e. to initially increase the concentration), and suppress them when they are not (i.e. to preferentially release non-target particles).

In addition to using simulations to explore different time-varying operating conditions, we also investigated cases where one type of physical coupling was entirely suppressed. Although both electrostatic and hydrodynamic interactions are involved in the dynamics of particle aggregates, we observed that hydrodynamics appear to play a particularly important role in separations. In the absence of hydrodynamic coupling, the particles freeze into a static arrangement if the addition of more particles is stopped (Figure 1*e*, Supporting movie S3). This is in strong contrast to our experimental observations, where we see arrangements of particles that are continually dynamic, reorganizing into different configurations (Figure 1*b*-*d*). This is a feature of dynamical frustration[22, 24], in which a system continually samples different states and is unable to reach a stable equilibrium. One source of dynamical frustration is an energy landscape with a well-defined global minimum but containing many local minima in which the system may become trapped[22, 37]. In the present context, interactions between neighboring particles within an aggregate give rise to a large number of local energy minima in which particles may be retained, despite the possible existence of more favorable (but inaccessible) states. Convergence to the global minimum depends in part on the rate at which alternate arrangements of particles are sampled. Because hydrodynamic interactions cause aggregates of particles to recirculate and sample a large number of configurations that would be inaccessible in a static, "frozen" system, they may play an important role in separating distinct components from a tightly interacting aggregate.

To test this idea, we performed simulations of separations (similar to those in Figure 4), but with (1) both hydrodynamic and electrostatic interactions, (2) only hydrodynamic interactions, or (3) only electrostatic interactions (Figure 5). As noted previously, we observed much more dynamic arrangements of particles with hydrodynamic interactions than without; in the case where only electrostatic interactions are included, the particles do not recirculate at all. Interestingly, the degree to which the particles recirculate appears to correlate with the predicted purity and recovery of the separations; for simulations including hydrodynamic interactions alone and those including combined hydrodynamic and electrostatic interactions, purity and recovery are similar (Figure 5*a*&*b*). For example, when changing polarizability (Figure 5*a*), we obtained 100% recovery when including HD+ES interactions and 90±8% recovery when only considering HD interactions, and the purities were also similar (74±7% and 66±16%, respectively). In contrast, simulations of separations including only electrostatic interactions show substantially lower recovery (47±18%), especially when the voltage is varied (Figure 5*b*) rather than the polarizability (Figure 5*a*). This is consistent with the hypothesis that static arrangements of particles are less able to decouple than dynamic arrangements, supporting the importance of hydrodynamic frustration in determining the performance of a separation when high concentrations of particles are used. Although we have arrived at this conclusion in the context of dielectrophoresis, it may reflect a general distinction between interaction forces that depend essentially on the *position* of a particle (electrostatics, in this case) as opposed to those that depend on both position and velocity. Accordingly, overlooking velocity-dependent interactions – more so than those only depending upon the position of particles - may lead to significant inaccuracies in the design or operation of microfluidic devices.

The performance of microfluidic devices for manipulating suspensions of cells or particles can vary considerably depending upon the concentration of the suspension and the mechanism through which the particles interact. This effect has been recognized in a wide variety of contexts, and in some cases has been experimentally characterized. Gascoyne *et al.*[38] reported a decrease in separation recovery from >90% to 10% over a 25-fold increase in cell concentration using dielectrophoretic field-flow fractionation, and Laurell *et al.* reported a quantitatively similar reduction in separation efficiency with increasing particle concentration using an acoustophoretic device[39]. In other instances where the concentration dependence is not specifically characterized, particle interactions are often cited as a likely source of discrepancy between modeling and experiments[40], or as motivation for operating at low particle concentrations[41]. Although this illustrates that an awareness of the potential implications of particle

interactions is widespread, the results presented here emphasize the richness of behavior that can arise through these interactions, and show that by studying them in more detail than is traditional, it is possible to arrive at insight into ways to improve separation performance.

To illustrate how the current work can be applied to one of these real-world applications, we performed a case study to investigate how particle interactions affect the performance of a simple system for DEP-FFF, and how simulations of these interactions might be used to optimize strategies for separations. Using a simplified two-dimensional model of a DEP-FFF flow cell, we simulated binary mixtures of cell-sized particles (radius of 6 μm, density of 1.06 g/l) at different concentrations and determined how the separation purity varies with concentration under different operating conditions. In these simulations (Figure 6), we vary the voltage and particle polarizability (K_1 and K_2 for the two different components of a binary mixture) so as to maintain constant equilibrium heights for particles in the flow cell. For a given concentration, the mixture will approach its equilibrium more ideally for $|K| \rightarrow 0$ (Figure 6*a*); as in the example of Figure 4, this corresponds to a suppression of electrostatic interactions, visible in the reduced tendency of particles to form chains aligned to the electric field in the lower panels of Figure 6*a*.

Interestingly, this sensitivity to polarizability is not uniform across concentration. Figure 6*b* gives average elution profiles for sequences of simulations with different concentrations (N = 4, 50, or 100 particles) and operating conditions. While in all cases, purity of the collected sample decreases with increasing concentration, the sensitivity to particle polarizability (and thus electrostatic interactions) is only pronounced at the intermediate concentration (N = 50). This suggests that the performance at the highest concentration (N = 100, where the purity ranges from 74-76%) is limited by steric constraints rather than any electric-field-induced aggregation. This simplified model of a real-world application captures a trend reported in the literature and emphasizes the potential subtlety of optimizing performance across a wide range of cell or particle concentrations.

Discussion

Although we have focused in our analysis on dielectrophoretic systems, and interactions may be simpler to describe in some separation methods and geometries than in others, we believe several results from this work should apply very generally. One of these is that an operating concentration that is "infinitely dilute" may be experimentally inaccessible in many cases. Even for suspensions with large characteristic distances between particles, statistical fluctuations in local particle concentration can give rise to strong interactions that propagate over space and time. This is illustrated (and described quantitatively) by the nucleation model we propose, characterized by the dramatic decrease in the threshold for trapping we observe as the particle concentration increases from zero (Figure 2*b*). The generality of this model – it does not invoke any assumptions specific to dielectrophoresis - suggests that it should apply regardless of the specific forces used to manipulate particles.

A second result that is applicable to a wide variety of separation methods (even those which do not specifically use microfluidics) is the idea of using time-varying operating conditions to improve separation performance. An analogy can be made between this approach to particle separation and existing DNA separation methods using time-varying operating conditions. For example, in pulsed-field electrophoresis[42,43], a time-varying electric field is used to separate large DNA molecules that would migrate at the same rate in a constant electric field. While in this case, the time-varying operating conditions act to overcome interactions of large molecules with themselves, for interacting colloidal systems, the effect is to modulate interactions of the particles with each other. This concept can be leveraged in any system where the interactions between particles are coupled to the external forces, a condition that holds for dielectrophoretic, electrophoretic, magnetic, and acoustic separations, in addition to any application where hydrodynamics are prominent. In these systems, changing the operating conditions (over space or time) as the concentration of particles changes (also over space or time) can

serve as a means of preferentially controlling the strength of interactions. In dielectrophoresis, we have demonstrated this concept by comparing separations with time-varying voltages and time-varying polarizability: separation methods that vary polarizability offer better control over particle interactions, owing to the different scaling of external ($\sim K$) and interaction ($\sim K^2$) forces with this parameter.

Although many types of particle interactions are coupled to the external forces in a system, an important distinction must be made regarding those that are not. While in the former case, time-varying operating conditions can be used to improve separation perfomance by exploiting cooperative effects to aid in the initial retention of particles without interfering with their eventual elution, this is not the case if interactions are driven entirely by the properties of the particles themselves and thus cannot be dynamically modulated. One universally important example is steric or excluded-volume interactions: if particles become too closely coupled through these mechanisms (or, in an extreme case, stick together through van der Waals or hydrophobic forces), separation performance will sharply diminish. As a result, there is an inevitable upper bound at which performance begins to decrease with particle concentration. Although where this upper bound lies will depend on factors we have not considered here (*e.g.* the surface properties of the particles), this question could be addressed, for example, by including short-range isotropic attractive forces to model the stickiness of cells, or relaxing steric constraints to approximate the effects of deformation. Understanding the interplay between induced and intrinsic interactions among particles will further aid in the development of new separation techniques that leverage a quantitative understanding of particle interactions to improve performance.

Materials and Methods

Device Fabrication, Packaging and Preparation. Electrodes for the microfluidic devices were fabricated on 6" Pyrex wafers using e-beam evaporation (2000-Å Au/100-Å Ti adhesion layer) and a standard liftoff process. Final electrode spacing and line width are 55 μm and 45 μm, respectively. For the microfluidic channels, we use PDMS replica molding from an SU-8 patterned silicon master (SU-8 2015, Microchem, Newton MA) to create channels with a width of 2 mm and a height of from 18 μm, achieving ~5% uniformity in film thickness over the area of the wafer. Electrical signals are created by a function generator (33220A, Agilent, Palo Alto, CA) and monitored by an oscilloscope (Tektronix, Richardson, TX). To make fluidic connections between the device and a syringe pump (KD Scientific 200, Holliston, MA), we use Tygon tubing (ID 0.02", OD 0.06", VWR, Brisbane, CA) press fit into the PDMS.

Numerical simulations. The first-order equations of motion appropriate for particles in a viscous medium (equations 1-3) are implemented in MATLAB® (MathWorks, Natick, MA) and solved through the numerical integration of equation 3 with respect to time. For the hydrodynamic and electrostatic Green's functions, we use stokeslet and dipole fields, respectively, along with the method of reflections to account for the boundaries of the microfluidic channel. In addition, we approximate near-field hydrodynamics using lubrication forces, as described in reference 35.

Particle aggregation experiments. To observe the dynamics of particles as they aggregate, we used a microfluidic channel with a height of 18 μm bonded to interdigitated electrodes with electrode width and pitch of 50 μm. We used particles of diameter 1.6 μm and 4 μm, as specified in Figure 1*b-d*, and applied voltages of 7-10 V_{pp} at 10 MHz. We generate and control the hydrodynamic fields using a syringe pump (KD Scientific, Holliston, MA), and set the flow rate to produce a depth-averaged fluid velocity of ~50-100 μm/s.

Particle characterization. In all experiments, we use polystyrene beads (09719, Polysciences, Inc. Warrington, PA, 1.646 ± 0.069 μm true diameter; F-8819 and F-8825, Molecular Probes Eugene, OR, 1.0 and 2.0 μm true diameters, respectively, ~1% CV estimated by manufacturer) suspended in a medium with a conductivity of 0.5 mS/m adjusted to the density of polystyrene using sucrose; to determine the

polarizability of particles in this medium, we first determined the particles' effective conductivities using crossover frequency measurements. For the particles displayed in Figure 5, these measurements (fitted to a single shell surface conductance model) predict polarizabilities of approximately -0.48 and -0.36 for the 1.6 μm green fluorescent beads and -0.46 and 0 for the 1.0 μm red fluorescent beads at frequencies of 10 MHz and 1 MHz, respectively. We control flowrates in the microfluidic device using a syringe pump set to generate an average fluid velocity of 45 μm/s, except where stated otherwise.

Fluorescence imaging. To determine the threshold for particle nucleation (Figure 2*b*), we use fluorescent microscopy to visually inspect the area of the device over which the external force is applied. After activating the electrodes at a particular voltage, we wait five minutes before inspecting the field for the presence of particle aggregates. To find the voltage threshold, we repeat this process at a lower or higher voltage until upper and lower limits on the threshold within 1 V of each other are determined (this corresponds to the error bars in Figure 2*b*).

To track the formation and dissociation of particle clusters (as in Figure 2*c* and Figure 4), we use the intensity of the fluorescent signal under constant imaging conditions to quantify the change in composition of the aggregate over time. For separations (Figure 3), we allow a mixture of particles to form an aggregate prior to introducing a step change in either voltage or frequency. Because we are only able to record images from one fluorescent channel at a time, during the period of dissagregation, we image those particles (1.0 μm red fluorescent beads in Figure 3) which we expect to be preferentially released from the cluster. Before and after dissagregation, we image from the alternate channel (in this case, the 1.6 μm green fluorescent beads).

Acknowledgements
This work was supported in part by NIH IDBR grant EB005753 and NSF grant DBI-0852654, and the Singapore-MIT Alliance.

Author Contributions
Both authors planned the research and contributed to data analysis and manuscript preparation. M.D.V performed experiments and simulations.

Competing Financial Interests
The authors declare no competing financial interests.

1 P. R. C. Gascoyne and J. Vykoukal, *Electrophoresis*, 2002, **23**, 1973.
2 J. Voldman, *Annual Review of Biomedical Engineering*, 2006, **8**, 425.
3 M. Prakash and N. Gershenfeld, *Science*, 2007, **315**, 832.
4 M. J. Fuerstman, P. Garstecki, and G. M. Whitesides, *Science*, 2007, **315**, 828.
5 M. Schindler and A. Ajdari, *Physical Review Letters*, 2008, **100**, 044501 [4 pages].
6 R. Tornay, T. Braschler, N. Demierre, B. Steitz, A. Finka, H. Hofmann, J. A. Hubbell, and P. Renaud, *Lab on a Chip*, 2008, **8**, 267.
7 K. J. Morton, K. Loutherback, D. W. Inglis, O. K. Tsui, J. C. Sturm, S. Y. Chou, and R. H. Austin, *Lab on a Chip*, 2008, **8**, 1448.
8 N. G. Green, A. Ramos, and H. Morgan, *Journal of Physics D: Applied Physics*, 2000, **33**, 632.
9 N. Pamme, *Lab Chip*, 2006, **6**, 24.
10 D. G. Grier, *Nature*, 2003, **424**, 810.
11 P. S. Doyle, J. Bibette, A. Bancaud, and J. L. Viovy, *Science*, 2002, **295**, 2237.
12 D. Di Carlo, *Lab Chip*, 2009, **9**, 3038.
13 M. Cross and P. Hohenberg, *Review of Modern Physics*, 1993, **65**, 851.
14 H. Swinney, 'Emergence and evolution of patterns', ed. V. Fitch, D. Marlow, and M. Dementi, Princeton University Press, 1997.
15 A. Turing, *Bulletin of Mathematical Biology*, 1990, **52**, 153.
16 K. A. Dill, K. M. Fiebig, and H. S. Chan, *Proc Natl Acad Sci U S A*, 1993, **90**, 1942.
17 R. Kikuchi, *Physical Review Letters*, 1951, **81**, 988.
18 M. F. Perutz, *Nature*, 1970, **228**, 726.
19 M. S. Z. Kellermayer, S. B. Smith, H. L. Granzier, and C. Bustamante, *Science*, 1997, **276**, 1112.
20 A. Pikovsky, M. Rosenblum, and J. Kurths, 'Synchronization: A Universal Concept in Nonlinear Science', Cambridge U. P., 2002.
21 S. H. Strogatz, *Nature*, 2001, **410**, 268.
22 J. N. Onuchic, Z. Luthey-Schulten, and P. G. Wolynes, *Annual Review of Physical Chemistry*, 1997, **48**, 545.
23 J. D. Bryngelson and P. G. Wolynes, *Proc Natl Acad Sci U S A*, 1987, **84**, 7524.
24 P.-M. Binder, *Science*, 2008, **320**, 322.
25 B. Khusid and A. Acrivos, *Physical Review E*, 1996, **54**, 5428 LP.
26 B. Khusid and A. Acrivos, *Physical Review E*, 1995, **52**, 1669.
27 D. J. Bennett, B. Khusid, C. D. James, P. C. Galambos, M. Okandan, D. Jacqmin, and A. Acrivos, *Applied Physics Letters*, 2003, **83**, 4866.
28 N. Aubry and P. Singh, *Electrophoresis*, 2006, **27**, 703.
29 E. R. Dufresne, T. M. Squires, M. P. Brenner, and D. G. Grier, *Physical Review Letters*, 2000, **85**, 3317.
30 P. Y. Chiou, A. T. Ohta, and M. C. Wu, *Nature*, 2005, **436**, 370.
31 M. Vahey and J. Voldman, *Analytical Chemistry*, 2008, **80**, 3135.
32 T. B. Jones, 'Electromechanics of Particles', Cambridge University Press, 1995.
33 J. Happel and H. Brenner, 'Low Reynolds Number Hydrodynamics: With Special Applications to Particulate Media', Kluwer, 1983.
34 D. L. Ermak and J. A. McCammon, *J. Chem. Phys.*, 1978, **69**, 1352.
35 J. F. Brady and G. Bossis, *Annual Review of Fluid Mechanics*, 1988, **20**, 111.
36 J. R. Blake and A. T. Chwang, *Journal of Engineering Mathematics*, 1974, **8**, 23.
37 H. Shintani and H. Tanaka, *Nature Physics*, 2006, **2**, 200.
38 P. R. C. Gascoyne, J. Noshari, T. J. Anderson, and F. F. Becker, *Electrophoresis*, 2009, **30**, 1388.
39 A. Nilsson, F. Petersson, H. Jonsson, and T. Laurell, *Lab Chip*, 2004, **4**, 131.
40 J. P. Beech, P. Jonsson, and J. O. Tegenfeldt, *Lab Chip*, 2009, **9**, 2698.
41 K. Smistrup, O. Hansen, H. Bruus, and M. F. Hansen, *Journal of magnetism and magnetic materials*, 2005, 597.
42 D. C. Schwartz and C. R. Cantor, *Cell*, 1984, **37**, 67.

43 J. M. Deutsch, *Phys Rev Lett*, 1987, **59**, 1255.

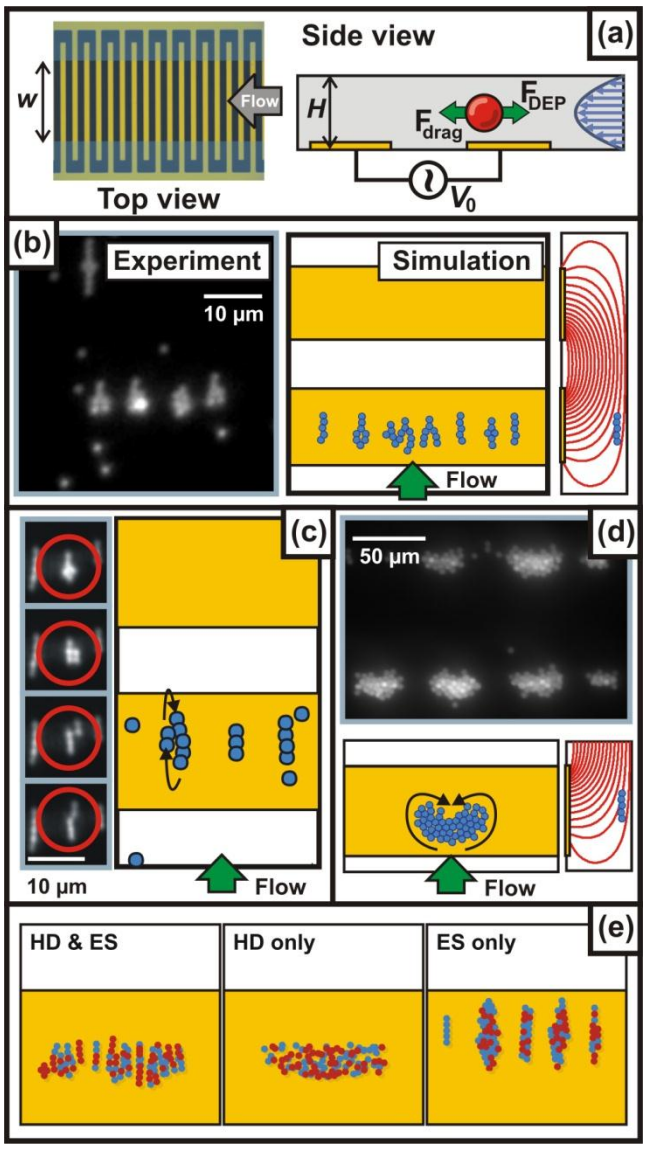

Figure 1: Emergent behavior of particle suspensions subjected to electric and hydrodynamic fields. (*a*) The device consists of an array of interdigitated electrodes and an overlaying microfluidic channel. (*b*) Examples of static "wishbone" shaped particle clusters, observed experimentally and predicted by simulations with electrostatic and hydrodynamic interactions (particle diameter 1.6 μm). (*c*) Longer chains of polarized particles exhibit a treadmilling instability, in which particles from the weakly polarized back end of the chain periodically dissociate and flow forward, where they rejoin the chain (particle diameter 1.6 μm). (*d*) Larger aggregates of particles form clusters which are driven by hydrodynamic coupling to continually recirculate (particle diameter 4.0 μm). (*e*) Simulations of aggregates containing ~100 particles with different types of interactions either active or suppressed ('HD' denotes hydrodynamic interactions, 'ES' denotes electrostatic interactions). Different colors (red and blue) are to emphasize internal organization (particle diameter 1.6 μm).

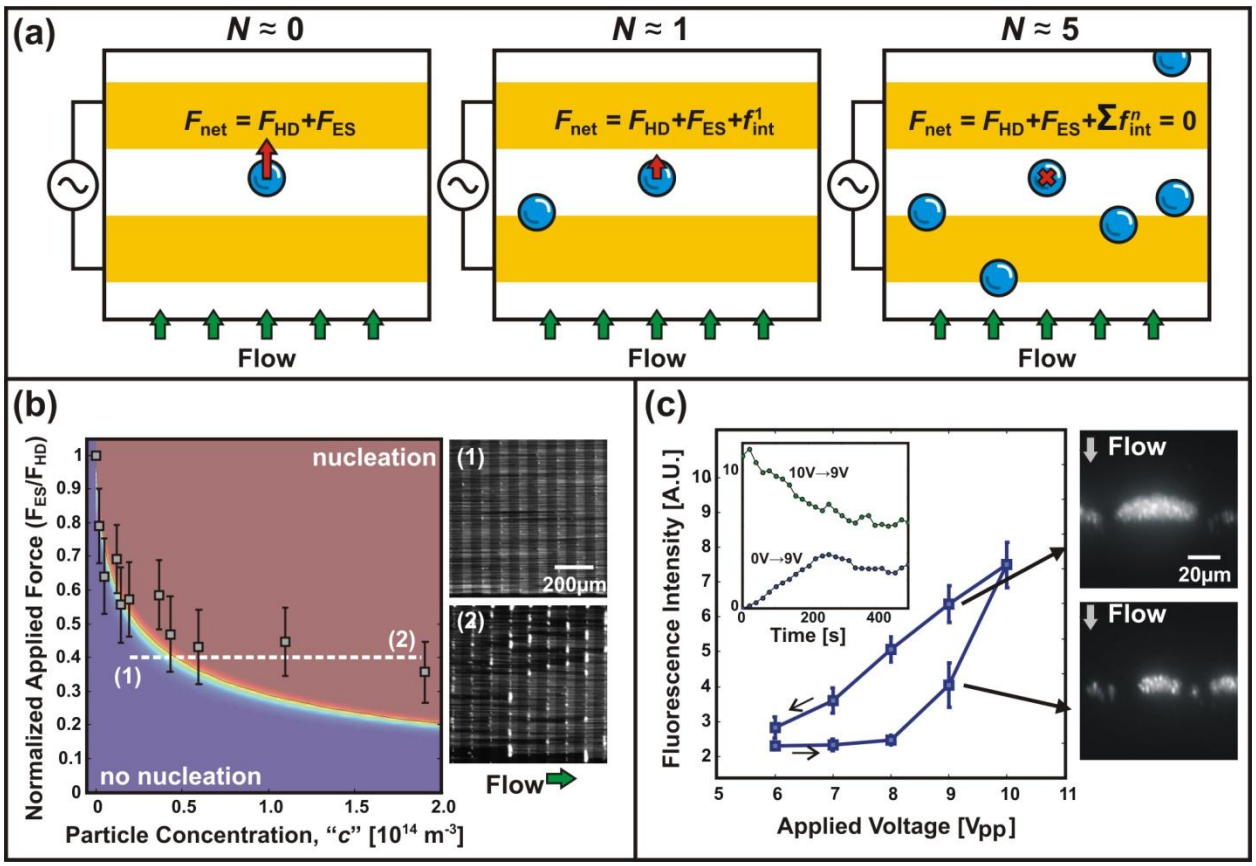

Figure 2: Nucleation of particle aggregates and hydrodynamic cooperativity. (*a*) Schematic of the model for nucleation through hydrodynamic interactions. A particle interacting with N of its nearest neighbors (N = 0, 1, 5, in the panels illustrated here) experiences an external force (F_{HD} + F_{ES}) in addition to an interaction force comprised of contributions from each of its neighbors (f^{n}_{int}). Statistical fluctuations in both N and f give rise to nucleation events in cases where F_{ES} alone would not otherwise be strong enough to retain particles against the fluid force F_{HD}. (b) A plot of the force-concentration threshold for nucleation events. The boxes indicate experimentally determined force thresholds (proportional to the square of the voltage threshold) for retaining particles while the dashed line gives the model prediction. Error bars represent upper and lower limits of the threshold forces (see Materials and Methods). The images (1) and (2) to the right show electrodes after 5 minutes of operation at identical voltages but ~10-fold difference in concentration, illustrating the onset of nucleation at high particle concentrations.. (*c*) A plot of particle retention (measured via fluorescence intensity; particle diameter of 1.6 μm) as applied voltage is varied, demonstrating hysteretic behavior in interacting particle systems, with arrows indicating the direction of traversal around the loop. The images to the right show steady-state particle aggregates at after the voltage is adjusted to 9 volts from below (8V → 9V) and above (10V → 9V). The inset shows the convergence to different steady-state concentrations when the steady-state voltage is approached from below (from 0V to 9V) or above (from 10V to 9V). Error bars in (*c*) represent s.d. for two independent experiments.

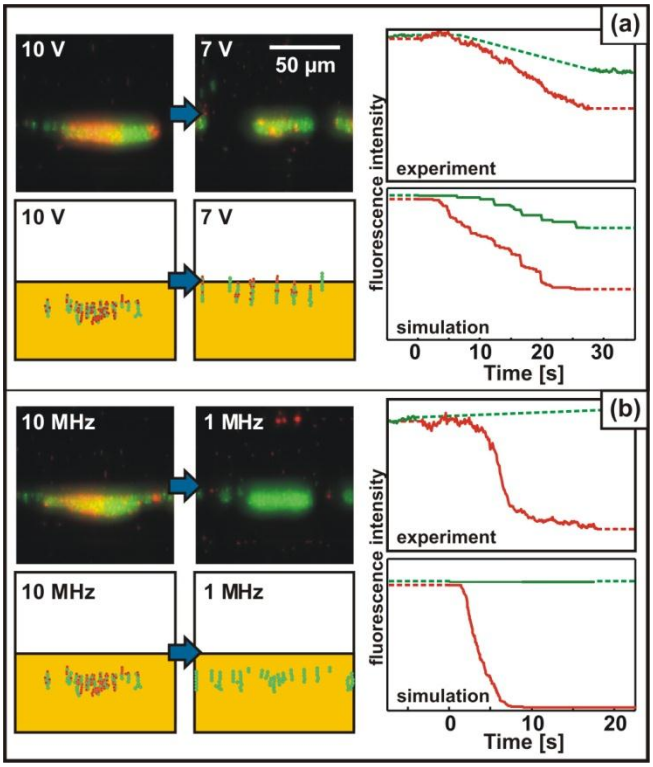

Figure 3: Dissociation of particle aggregates under dynamic operating conditions. (*a*) Experiments and simulations in which the voltage is decreased (from 10 V to 7 V), showing the initial and final states of the cluster (left) and the dynamics of dissociation (right). In both experiments and simulations, the decreased voltage intended to separate out the red particles while retaining the green particles. (*b*) Same as (*a*), except the frequency is varied; separation in this case is more rapid and results in higher purity. Dashed lines give interpolations of intensity for intervals during which the opposite (either red or green) channel was imaged.

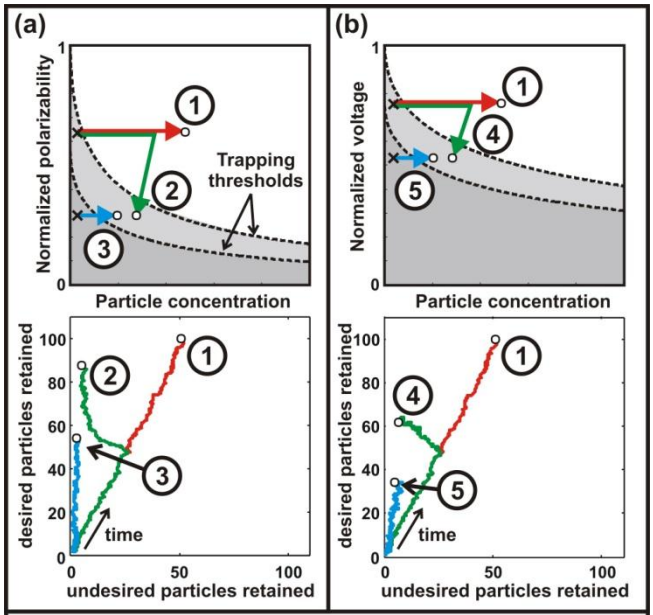

	Initial Condition		Final Condition		Force Ratio (Final:Initial)		Purity	Recovery
	V	K_1	V	K_1	f_{int}	f_{ext}		
①	9	-0.5	9	-0.5	1	1	66 ± 2%	100%
②	9	-0.5	9	-0.2	0.19	0.44	96 ± 2%	88 ± 3%
③	9	-0.2	9	-0.2	1	1	98 ± 4%	55 ± 7%
④	9	-0.5	6	-0.5	0.44	0.44	90 ± 5%	62 ± 15%
⑤	6	-0.5	6	-0.5	1	1	89 ± 9%	35 ± 6%

Figure 4: Leveraging dynamic operating conditions to improve separation performance. The top panels in (*a*) and (*b*) show the trapping thresholds (dashed lines) for binary separations using polarizability (in *a*) and voltage (in *b*). The operating conditions are either maintained constant ('1', '3', and '5'), or changed midway through the separation ('2' and '4'). The bottom panels in (*a*) and (*b*) give simulation results for number of particles retained when 100 desired particles and 100 undesired particles are introduced into the system at a concentration of ~0.3×10^{14} m^{-3} (a volume fraction of 0.03%). By tracking the number of each particle type retained as the separation evolves (the number of particles increases over time from an initial value of zero), we generate the curves shown. The table in (*c*) summarizes the results (averaged over 10 simulations for each condition). Continual operation in state '1' results in poor separation purity, while continual operation in states '3' or '5' results in poor recovery; overall performance is improved by changing the operation conditions midway through the separation.

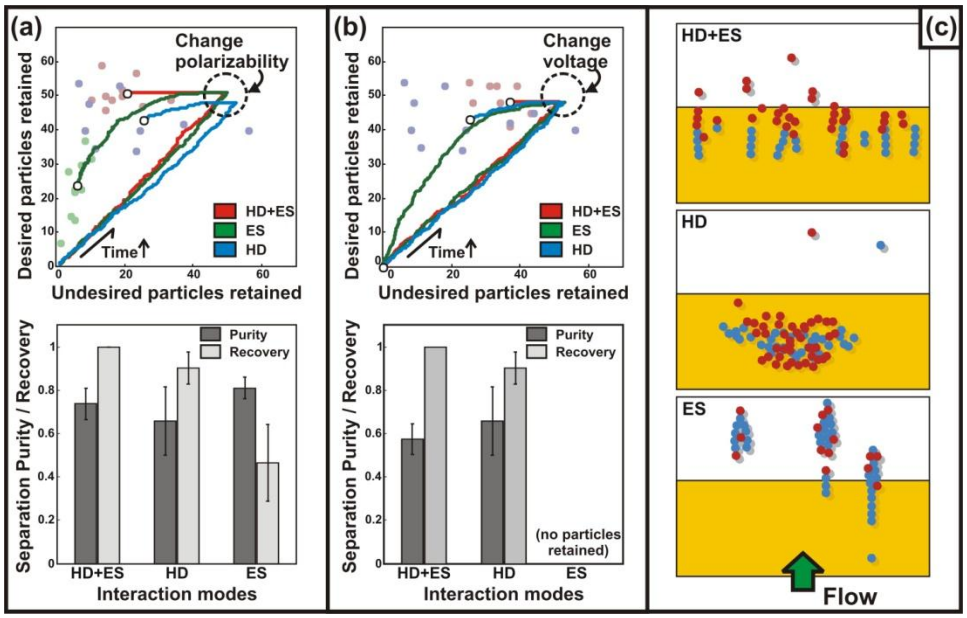

Figure 5: Simulations of binary separations with various combinations of interaction modes (hydrodynamic = 'HD'; electrostatic = 'ES') active or suppressed. (a) Separations where the electrical force is varied through the particles' polarizabilities. In each simulation, 100 particles are introduced at a concentration of ~1×10^{14} m^{-3} (a volume fraction of 0.1%, ~3× higher than the simulations in Figure 3) prior to decreasing the external electrical force by ~44%. Bar plots give the purity and recovery determined from the final numbers of desired and undesired particles retained, averaged over ten simulations. Simulations including only hydrodynamic interactions ('HD') have similar outcomes to those including both hydrodynamic and electrostatic interactions ('HD + ES'). Including electrostatic interactions only ('ES') results in substantial loss of both desired and undesired particles when the field is reduced. (b) Similar to (a), except with the external electrical force varied by changing the voltage. Here, inclusion of electrostatic interactions only results in the loss of all particles, in contrast to the corresponding simulation from (a); this follows from the different scaling of external and interaction forces with polarizability and voltage. (c) Images from simulations of dissagregating particle clusters for the three types of simulations. Although the outcome (*i.e.* purity and recovery) is similar for 'HD + ES' and 'HD' simulations, the spatial arrangements of particles are quite distinct.

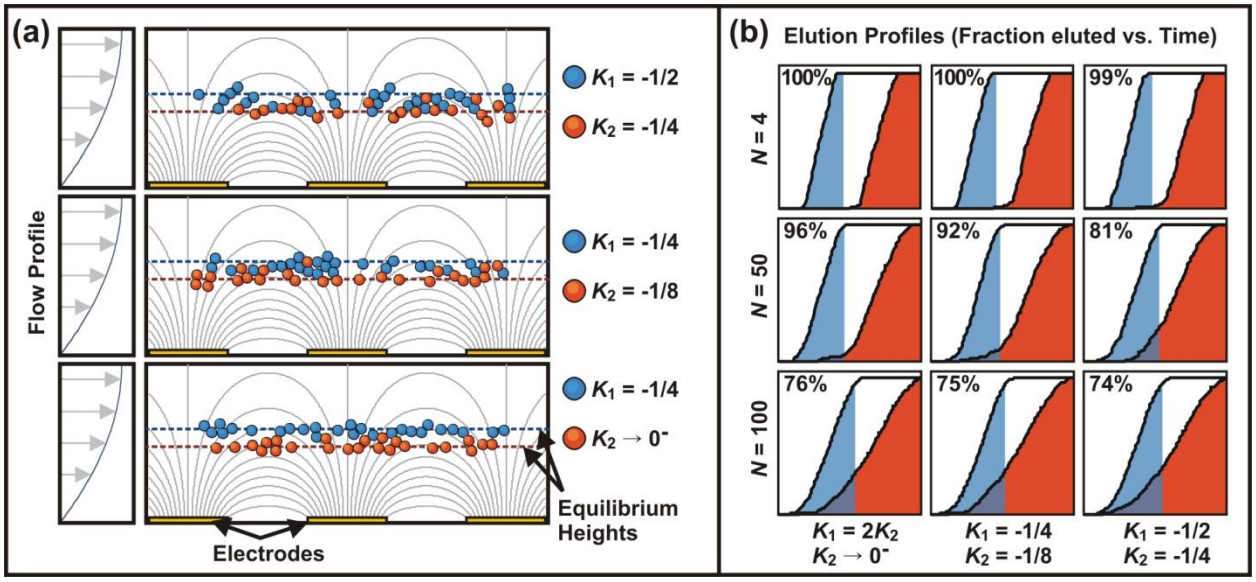

Figure 6: Particle interactions in DEP-FFF. (*a*) A portion of the DEP-FFF flow cell, viewed from the side. A binary particle mixture is levitated to equilibrium before starting flow to elute the particles. For a given particle concentration (N = 50 in this case), decreasing the particle polarizabilities (K_1 and K_2) while increasing the voltage to maintain constant equilibrium heights (indicated by the dashed horizontal lines) results in more idealized convergence to equilibrium (note, for example, the reduced chain formation in the lower panel relative to the upper panel). (*b*) Plots showing the fraction of particles eluted vs. time for a binary mixture. The blue shading indicates the time during which the first particle type is collected, resulting in the purity given in the upper left corner. While increasing the concentration (N) reduces the purity in all cases, only the intermediate concentration (N = 50) is sensitive to the operating polarizability (with purity decreasing from 96% to 81% at varying K, whereas purity is almost constant across K for N=4 and N=100), suggesting that at this concentration, performance is limited by electrostatic interactions, whereas at high concentrations (N = 100) steric interactions are limiting.